Chapter 4

AXIAL-FLOW COMPRESSOR BLADE PROFILES

The traditional approach to axial-flow compressor aerodynamic design was to use various families of airfoils as the basis for blade design. American practice was based on various families defined by the National Advisory Committee for Aeronautics (NACA), the most popular being the 65-series family. British practice often centered about the C-series families, using circular-arc or parabolic-arc camberlines. As design requirements began to favor transonic operation, double-circular-arc blades became popular. The performance characteristics of these airfoil families are well understood due to extensive experimental cascade testing, much of which is available in the literature.

In recent years, use of blades designed for a prescribed surface velocity distribution or blade loading style, instead of for predefined airfoil families has become popular. Often, inverse design methods that predict the blade shape required for the desired blade loading are used. As the relation between blade shape and preferred loading styles became better understood, it also became common to use conventional or direct analysis methods in a trial-and-error mode to arrive at the same result. These airfoils have been referred to as prescribed velocity distribution (PDF) blades (Cumpsty, 1989), even though the term controlled diffusion airfoils is probably more common today. Although the literature offers general guidelines for these designs, the actual airfoil designs in use are proprietary. In general, the performance characteristics of these airfoils are well known only to the organizations that developed them.

As discussed in the preface to this book, this situation posed a significant complication to the goal of providing a complete description of the working design and analysis system. It was quickly recognized that it is no longer possible to write a book that can be directly applied to all of the many proprietary designs in use today. But this is not considered to be a serious limitation. In this writer's experience, the process of adapting classical blade performance prediction models to a more modern controlled diffusion airfoil design is not particularly difficult, assuming the performance characteristics of the airfoil are known.

This chapter provides a complete description of the more commonly used traditional airfoil families, and Chapter 6 provides a detailed description of the performance modeling for these same airfoil families. This ensures that this book is at least complete in the context of classical axial-flow compressor technology.

General concepts from the literature used to guide the development of controlled diffusion airfoils are also briefly reviewed in this chapter.

NOMENCLATURE

a = distance along chord to the point of maximum camber
b = distance normal to the chord line to the point of maximum camber
C_{l0} = isolated airfoil lift coefficient
c = chord length
d = length defined in Eq. (4-24)
i = incidence angle
o = blade throat opening
R = circular-arc radius of curvature
s = blade pitch (spacing)
t_b = blade maximum thickness
x = coordinate along the chord
y = coordinate normal to the chord
y_C = y coordinate at the origin of R_C
α = angle of attack
β = flow angle relative to axial direction
χ = blade angle relative to the chord line
δ = deviation angle
γ = stagger (setting) angle
κ = blade angle relative to the axial direction
θ = camber angle
σ = solidity
ϕ = parameter defined in Eq. (4-30)

Subscripts

C = camberline parameter
L = blade lower or pressure surface parameter
U = blade upper or suction surface parameter
1 = blade leading edge parameter
2 = blade trailing edge parameter

4.1 CASCADE NOMENCLATURE

Figures 4-1 and 4-2 illustrate the basic parameters used to describe axial-flow compressor blades and cascades. Blades are defined by a mean camberline, $y(x)$, upon which a profile or thickness distribution, $t_b(x)$, is imposed. The angles between slopes to the camberline and the chord line at the leading and the trailing edges are designated as χ_1 and χ_2, respectively. The blade camber angle is defined as

$$\theta = \chi_1 + \chi_2 \tag{4-1}$$

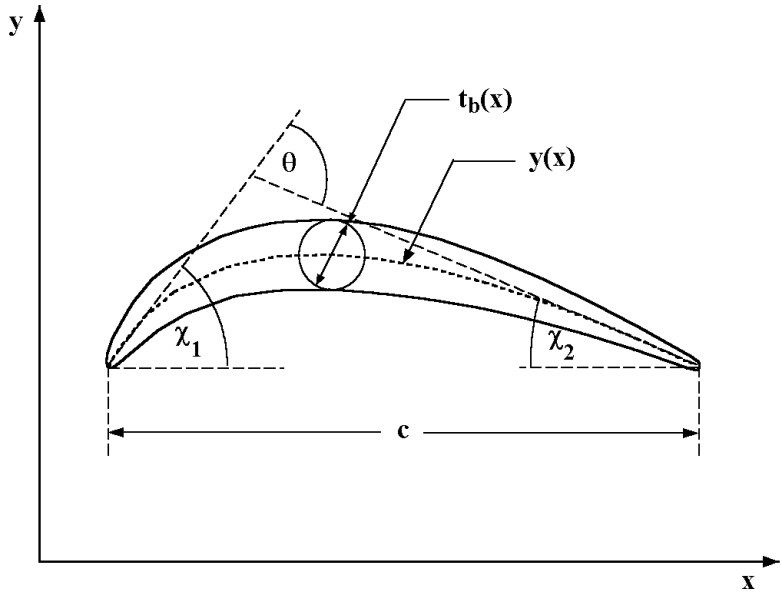

FIGURE 4-1 Basic Airfoil Geometry

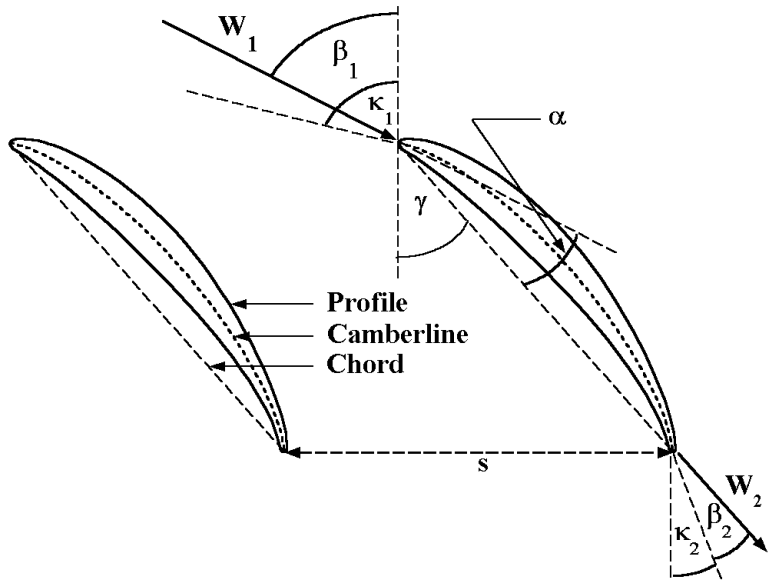

FIGURE 4-2 Basic Cascade Geometry

The pitch or the spacing between adjacent blades, s, and the chord length, c, define the cascade solidity, σ, by

$$\sigma = c / s \tag{4-2}$$

The angle between the chord line and the axial direction is referred to as the stagger angle, or setting angle, γ. The angle between the inlet velocity vector, W_1, and the chord line of the staggered blade is called the angle of attack, α. The flow angle with respect to the axial direction will be designated as β_1. The angles between slopes to the camberline and the axial direction at the leading and the trailing edges will be designated as κ_1 and κ_2, respectively. Similarly, the flow angle at the blade trailing edge will be designated as β_2. The flow incidence angle, i, the deviation angle, δ, and the angle of attack, α, are defined as

$$i = \beta_1 - \kappa_1 \tag{4-3}$$

$$\delta = \beta_2 - \kappa_2 \tag{4-4}$$

$$\alpha = \beta_1 - \gamma \tag{4-5}$$

This nomenclature is directly applicable to blades based on well-defined camberlines such as the circular-arc and parabolic-arc camberlines typical of British practice. American practice has often been based on blades derived from NACA aircraft wing airfoils, which typically have infinite camberline slopes at the leading and trailing edges. In those cases, parameters such as κ, χ, θ, i and δ lose significance unless a suitable approximate or reference camberline is used to define them. Common practice has been to use an equivalent circular-arc camberline as a reference for the NACA 65-series blades (Johnsen and Bullock, 1965). This writer has made similar use of an equivalent parabolic-arc camberline for the NACA A_4K_6 63-series guide vanes (Dunavant, 1957), where the point of maximum camber is not at mid-chord.

Construction of blades from the base camberline and profile has occasionally been a source of confusion. Profile thickness distributions are normally supplied for zero-camber blades as a function of distance along the chord, which also is the camberline for that case. When imposing a profile on a blade with camber, the thickness distribution data should be interpreted in terms of dimensionless distance along the camberline rather than along the chord line.

4.2 NACA 65-SERIES PROFILE

The NACA 65-series blades are derived from NACA aircraft wing airfoils designed for approximately uniform loading. The original aircraft wing airfoil was not structurally suitable for the compressor cascade application. There are a number of adaptations of the original profile thickness distribution in use. The profile reported by Emery et al. (1958) is representative of the basic NACA 65-series cascade profile. Table 4-1 provides the thickness distribution from that reference. Even that profile has been structurally suspect due to its sharp trailing edge, as

Table 4-1 Dimensionless Data for Standard Axial-Flow Compressor Blade Types

NACA 65-(10)10 Series			NACA A_4K_6 63 Series		C.4 Series
x/c ~ %	y/c ~ %	t_b/c ~ %	y/c ~%	t_b/c ~ %	t_b/c ~ %
0	0	0	0	0	0
0.5	0.250	1.544	0.376	——	——
0.75	0.350	1.864	——	——	——
1.25	0.535	2.338	0.792	1.542	3.30
2.5	0.930	3.480	1.357	2.114	4.54
5.0	1.580	4.354	2.248	2.924	6.16
7.5	2.120	5.294	——	——	7.24
10	2.585	6.080	3.531	4.020	8.04
15	3.365	7.332	4.420	4.772	9.10
20	3.980	8.286	5.040	5.312	9.66
25	4.475	9.006	5.458	5.682	——
30	4.860	9.520	5.710	5.908	10.0
35	5.150	9.848	5.824	6.000	——
40	5.355	9.992	5.820	5.942	9.78
45	5.475	9.926	5.713	5.754	——
50	5.515	9.624	5.516	5.446	9.14
55	5.475	9.060	5.239	5.034	——
60	5.355	8.292	4.891	4.602	8.10
65	5.150	7.364	4.479	4.170	——
70	4.860	6.312	4.011	3.740	6.74
75	4.475	5.168	3.492	3.308	——
80	3.980	3.974	2.922	2.876	5.08
85	3.365	2.770	2.308	2.444	——
90	2.585	1.620	1.642	2.014	3.20
95	1.580	0.612	0.912	1.582	2.12
100	0	0	0	0	0
R_{LE}/c ~ %	——	0.687	——	0.297	1.20
R_{TE}/c ~ %	——	0	——	0.600	0.60

well as it being very thin toward the trailing edge. Kovach and Sandercock (1961) describe a more satisfactory modification for use in compressors. They use the basic distribution from Table 4-1 up to 60% of the chord. Then the thickness is varied linearly to match a trailing edge radius equal to 0.8% of chord. It is likely there are many other variants on the 65-series profile that are in use for reasons of structural integrity. The base profile has its maximum thickness at 40% of chord.

NACA 65-series airfoils are designated by their lift coefficient and maximum thickness-to-chord ratio. The lift coefficient in tenths appears first in parentheses, followed by the thickness-to-chord ratio as a percentage. Hence a 10% thick airfoil with a lift coefficient of 1.5 is designated as NACA 65-(15)10. For lift coefficients less than one, the parentheses may be omitted. The base camberline is defined for a lift coefficient of 1.0 and is supplied in Table 4-1 (Emery et al., 1958). Simply multiply these coordinates by the lift coefficient to create other camberlines. Hence, the base airfoil for the NACA 65-series is the NACA 65-(10)10. Figure 4-3 illustrates this airfoil, using the base thickness of the NACA 65-010 from Table 4-1.

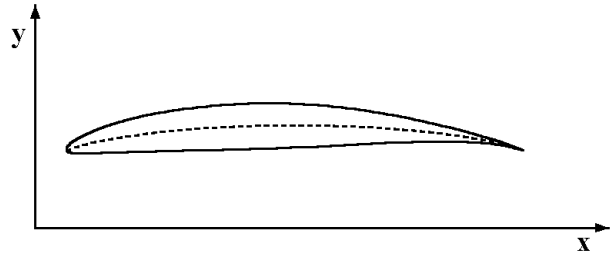

FIGURE 4-3 The NACA 65-(10)10 Airfoil

As noted, the slope of the NACA 65-series camberline becomes infinite at the leading and trailing edges. For this reason, experimental data from cascade testing are normally expressed in terms of angle of attack and fluid turning instead of incidence angle and deviation angle. It is now accepted practice to define effective inlet and discharge blade angles using an effective circular-arc camberline. The circular-arc is defined as that which passes through the end points and the point of maximum camber at mid-chord (Johnsen and Bullock, 1965). Figure 4-4 shows a comparison of the equivalent circular-arc camberline with the NACA 65-(12) camberline. The construction of the circular-arc camberline reviewed in the next section can be used for that purpose. Figure 126 of Johnsen and Bullock (1965) provides a

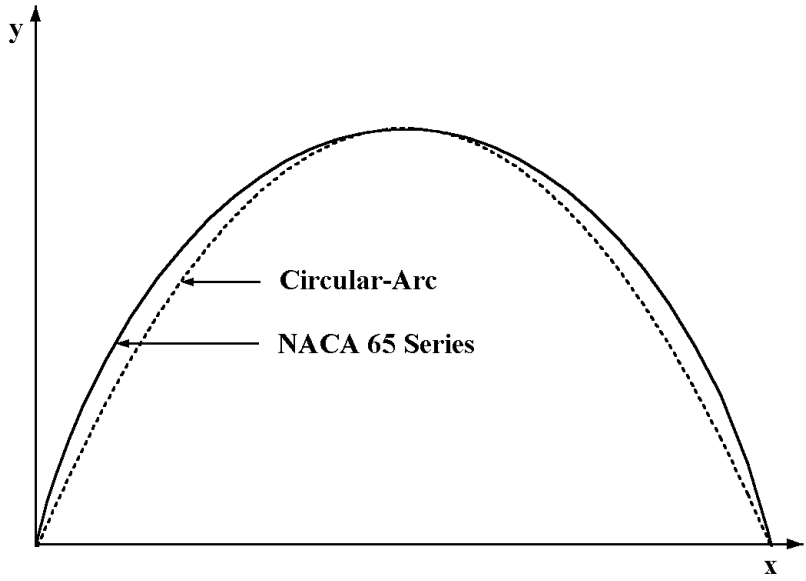

FIGURE 4-4 Equivalent Circular-Arc Camberline

graphical relation between the effective camber angle and the lift coefficient. As will be seen in the next section, C_{lo} and the equivalent θ can be related analytically by

$$\tan(\theta/4) = 0.1103 C_{lo} \tag{4-6}$$

4.3 CIRCULAR-ARC CAMBERLINE

The circular-arc camberline is commonly used in conjunction with the British C.4 series blade profile. It is also the camberline used for the double-circular-arc profile, and is reported to be used in place of the NACA 65-series camberline, when using the NACA 65-series profile (Cumpsty, 1989). As mentioned in the previous section, it is commonly used as an effective camberline for the NACA 65-series blades to provide a meaningful definition of the leading and trailing edge blade angles. This camberline is completely defined by the camber angle, θ, and chord length, c. Figure 4-5 illustrates its construction. The radius of curvature, R_C, of the camberline is given by

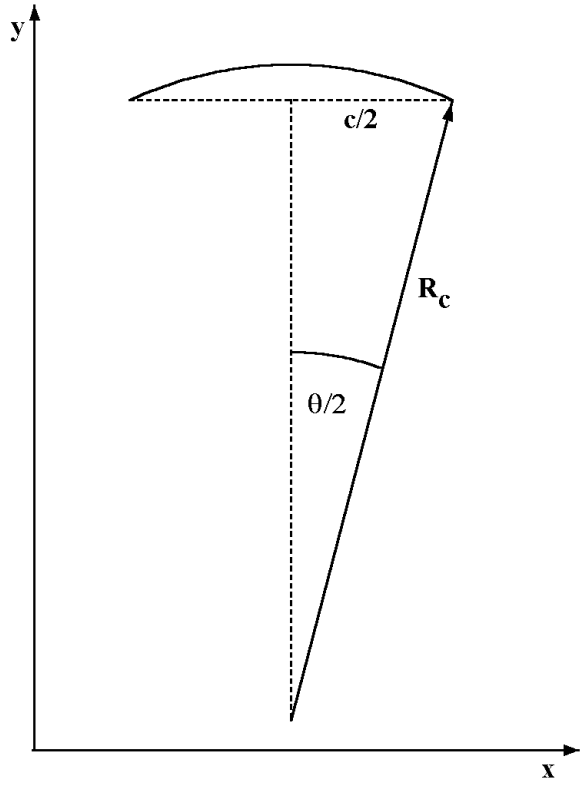

FIGURE 4-5 Circular-Arc Camberline Construction

$$c/2 = R_C \sin(\theta/2) \tag{4-7}$$

The coordinates of the origin of the radius of curvature are $(0, y_C)$, where

$$y_C = -R_C \cos(\theta/2) \tag{4-8}$$

Then, for any x from $-c/2$ to $c/2$,

$$y = y_C + \sqrt{R_C^2 - x^2} \tag{4-9}$$

Using Eqs. (4-7) and (4-8), the camberline coordinate, $y(0)$, at mid-chord can be expressed as

$$2y(0)/c = [1 - \cos(\theta/2)]/\sin(\theta/2) = \tan(\theta/4) \tag{4-10}$$

which is the basis for Eq. (4-6), where $y(0)/c = 0.05515$ is given in Table 4-1 and multiplied by C_{l0} to obtain the value for any lift coefficient.

4.4 PARABOLIC-ARC CAMBERLINE

The parabolic-arc camberline is also used with the British C.4 profile and can be used with other profiles as well. This writer has used it as an equivalent camberline to define effective blade angles for the NACA A_4K_6 63-series guide vane camberline. The parabolic-arc allows a more general blade loading style than the circular-arc. Front-loaded, mid-loaded and rear-loaded blades are all possible, depending on where the point of maximum camber is located. Figure 4-6 illustrates this blade style. The point of maximum camber is located at $x = a$ and $y = b$, which provides the basic definition of the camberline. The basic constraints to be satisfied are

$$y(0) = 0 \tag{4-11}$$

$$y(c) = 0 \tag{4-12}$$

$$y(a) = b \tag{4-13}$$

$$y'(a) = 0 \tag{4-14}$$

The camberline is generated using the general second-order equation for a parabola that is given in many standard mathematics references. It can be written as

$$Ax^2 + 2\sqrt{AE}xy + By^2 + Cx + Dy + E = 0 \tag{4-15}$$

There appears to be a problem since we have five coefficients but only four constraints. However, one of the coefficients is arbitrary, e.g., we can divide through

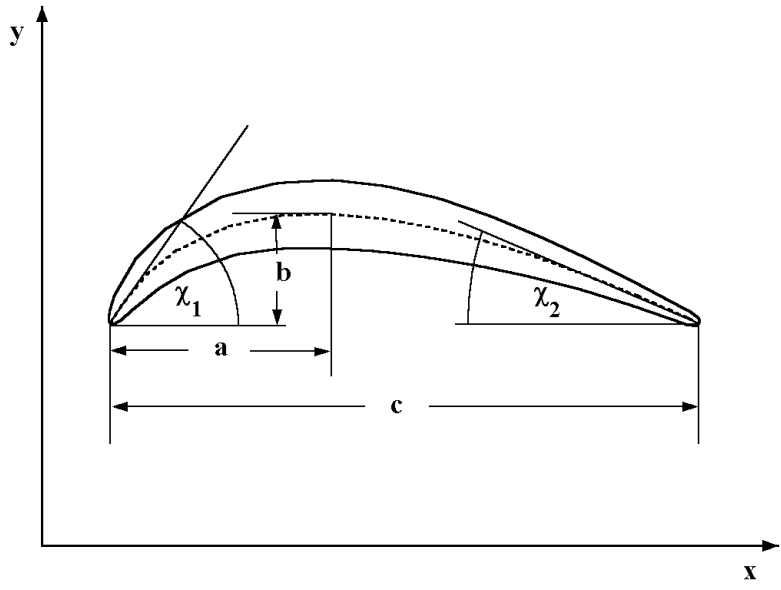

FIGURE 4-6 The Parabolic-Arc Camberline

the equation by B and eliminate it. Hence Eqs. (4-11) through (4-14) are sufficient to determine all coefficients in Eq. (4-15). The algebra is very tedious, but the result can be shown to be

$$x^2 + \frac{c-2a}{b}xy + \frac{(c-2a)^2}{4b^2}y^2 - cx - \frac{c^2-4ac}{4b}y = 0 \tag{4-16}$$

Normally, specification of the blade camber angle, θ, or the blade angles, χ_1 and χ_2, is preferred. Differentiating Eq. (4-16) and evaluating the derivatives at $x = 0$ and $x = c$ yields

$$\tan\chi_1 = 4b/(4a-c) \tag{4-17}$$

$$\tan\chi_2 = 4b/(3c-4a) \tag{4-18}$$

Equations (4-1) and (4-16) through (4-18) can be combined to yield.

$$b/c = \{\sqrt{1+(4\tan\theta)^2[a/c-(a/c)^2-3/16]}-1\}/(4\tan\theta) \tag{4-19}$$

This defines the parabolic-arc camberline in terms of camber and the ratio, a/c. For compressor blades, it is reasonable to restrict the leading and trailing edge angles to be less than 90°, i.e.,

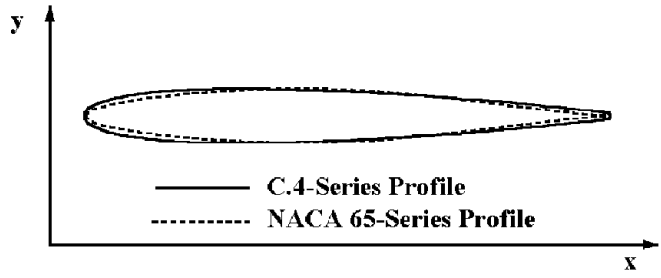

FIGURE 4-7 The C.4 and 65-Series Profiles

$$0.25 < a/c < 0.75s \tag{4-20}$$

For any value of x, Eq. (4-16) can be solved for y as a standard quadratic equation. This approach will be singular for $a/c = 0.5$, since two of the terms drop out. But that special case is a simple and direct solution. Both cases can be treated by a numerical recursion equation of the form

$$y = x(c-x)/[\frac{(c-2a)^2}{4b^2}y + \frac{c-2a}{b}x - \frac{c^2-4ac}{4b}] \tag{4-21}$$

Simply start with $y = 0$ and repeatedly solve this equation to converge on the correct value of y.

4.5 BRITISH C.4 PROFILE

The C.4 profile is one of several profiles in the British C-series (Howell, 1942). The C.4 series received the most attention in the literature relative to its performance characteristics (e.g., Johnsen and Bullock, 1965). Its base thickness distribution is tabulated in Table 4-1. Figure 4-7 shows an overlay of the C.4 and the NACA 65-series profiles. The C.4 profile is thicker toward the leading edge and has its maximum thickness at 30% of chord, compared to 40% for the 65-series profile. This would be expected to make it less effective for higher Mach number applications, but it would normally offer advantages relative to structural integrity. Similar comments apply to the trailing edge region. But, as noted, the 65-series profile is usually modified in that region. This profile is normally applied to circular-arc or parabolic-arc camberlines. It is reported that a later series, the C.7 profile, has seen more use in compressors and has many features in common with the 65-series profile (Cumpsty, 1989). C-series profiles are designated by a code giving the t_b, profile, θ, camberline and a/c. Hence, a 10C4/20P40 blade is a 10% thick C.4 profile with a 20° camber angle using a parabolic-arc camberline with $a/c = 0.4$. A 10C4/20C50 blade would be similar, but with a circular-arc camberline. This writer has not had direct experience with this profile,

but it is well-established and empirical performance prediction models do exist for its application. On the other hand, there really is no reason why the 65-series profile cannot be applied to the circular-arc and parabolic-arc camberlines. That approach would be expected to yield better performance, particularly at higher Mach numbers.

4.6 DOUBLE-CIRCULAR-ARC PROFILE

The double-circular-arc profile is constructed with both surfaces formed by circular-arcs, which blend with a nose radius, r_0, applied at both the leading and trailing edges. Designate the lower and upper surface arc radii of curvature as R_L and R_U, respectively, as illustrated in Fig. 4-8. The construction of the camberline, with a radius of curvature, R_C, has been described in Section 4.3. Here, construction of the upper surface of the profile will be illustrated. Construction of the lower surface is quite similar, except that certain parameters, such as t_b and r_0, are assigned negative values. The distance, Δx_U, from mid-chord to the center of the nose radius at the trailing edge is given by

$$\Delta x_U = (R_U - r_0)\sin(\theta_U / 2) = c/2 - r_0\cos(\theta/2) \tag{4-22}$$

where θ is the blade camber angle and θ_U is shown in Fig. 4-8. The distance, Δy_U, is given by

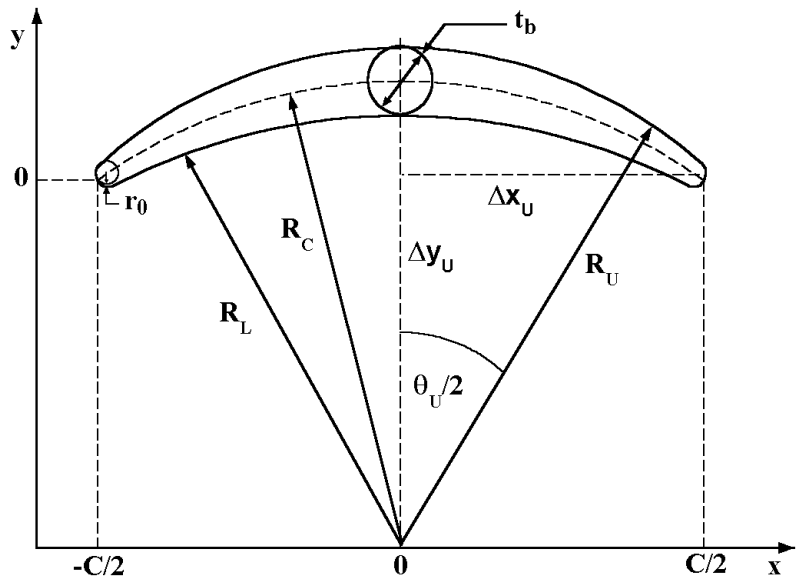

FIGURE 4-8 Double-Circular-Arc Profile

$$\Delta y_U = R_U - y(0) - t_b / 2 + r_0 \sin(\theta / 2) = R_U - d \tag{4-23}$$

where the camberline coordinate, $y(0)$, is given by Eq. (4-10) and d is defined as

$$d = y(0) + t_b / 2 - r_0 \sin(\theta / 2) \tag{4-24}$$

The Pythagorean theorem applied to the right triangle in Fig. 4-8 requires

$$[R_U - r_0]^2 = [R_U - d]^2 + [c / 2 - r_0 \cos(\theta / 2)]^2 \tag{4-25}$$

After some tedious algebra, this yields

$$R_U = \frac{d^2 - r_0^2 + [c / 2 - r_0 \cos(\theta / 2)]^2}{2(d - r_0)} \tag{4-26}$$

The upper surface circular-arc extends through polar angles from $-\theta_U / 2$ to $\theta_U / 2$, constructed using the radius of curvature, R_U, and the location of its origin at $x = 0$ and $y = y(0) + t_b / 2 - R_U$. The leading and trailing edge radii are constructed about their centers at $y = r_0 \sin(\theta / 2)$ and $x = \pm [c / 2 - r_0 \cos(\theta / 2)]$ to blend with the circular-arc.

4.7 NACA A_4K_6 63-SERIES GUIDE VANE PROFILE

Dunavant (1957) provides design and application data for a very effective vane profile for use as inlet guide vanes. This vane has excellent flow guidance and a wide incidence operating range. The camberline is developed by combining a front-loaded (A) profile with $C_{l0} = 0.4$ and a uniform-loaded (K) profile with $C_{l0} = 0.6$, which is designated as the A_4K_6 camberline corresponding to $C_{l0} = 1$. This is combined with the 6% thick NACA 63-series profile as the base guide vane geometry. The base camberline coordinates and thickness distribution are listed in Table 4-1 and illustrated in Fig. 4-9. Similar to the 65-series blades, the camberline coordinates can be scaled directly by lift coefficient to alternate camberlines. Similarly, the thickness distribution can be scaled to other values from the base 6% thick profile. The general vane designation is 63-(C_{l0} A_4K_6)nn, where nn is the maximum thickness as percent of chord. The maximum thickness of this vane is at 35% of chord. The location of the point of maximum camber can be estimated by interpolation to be at approximately $a / c = 0.375$ with $b / c = 0.0583$ for $C_{l0} = 1$. As is the case with the NACA 65-series camberline, the leading and trailing edge camberline slopes are infinite. Here, an equivalent parabolic-arc camberline can be used to allow viable definitions of leading and trailing edge blade angles, incidence angle and deviation angle. Equation (4-19) can be solved for camber angle to yield

$$\tan\theta = \frac{b / c}{2[a / c - (a / c)^2 - 3/16 - (b / c)^2]} \tag{4-27}$$

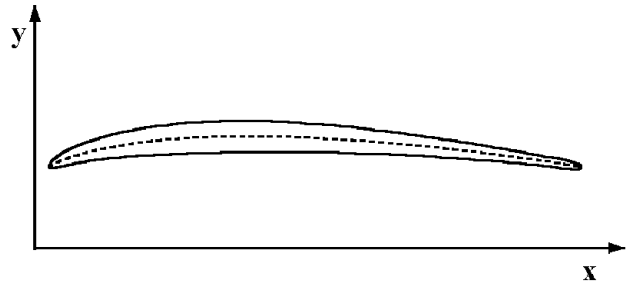

FIGURE 4-9 NACA 63-(10A_4K_6)06

Hence, for the A_4K_6 camberline,

$$\tan\theta = \frac{291.5C_{l0}}{468.75 - (5.83C_{l0})^2} \tag{4-28}$$

which yields $\theta = 33.8°$ at $C_{l0} = 1$. A simpler approximation is obtained by generalizing the equivalent circular-arc camberline conversion of Eq. (4-6) by dividing the right-hand side by $2a / c$ to yield.

$$\tan(\theta/4) = 0.05515C_{l0} / (a/c) \tag{4-29}$$

which yields $\theta = 33.5°$ at $C_{l0} = 1$. As long as only the NACA 65-series and A_4K_6 camberlines require conversion between θ and C_{l0}, this equation can be applied to either one. It also can be easily inverted for circular-arc and parabolic-arc camberlines to permit application of empirical blade performance correlations given as a function of C_{l0} to those camberline types.

4.8 CONTROLLED-DIFFUSION AIRFOILS

The standard blade profiles described in this chapter have been used extensively for axial-flow compressors. They are well understood, reliable and can yield excellent performance when properly applied. But, in recent years, many investigators have explored alternatives offering better Mach number range and higher efficiency. These are often referred to as controlled diffusion airfoils, since the design of the profiles is based on producing carefully controlled blade surface Mach number distributions.

Hobbs and Weingold (1984) and Dunker et al. (1984) have reviewed the basic design strategy. They indicate that the key features are:

- A continuous acceleration along the suction surface and near the leading edge to avoid laminar boundary layer separation or premature separation.

- The peak Mach number should not exceed 1.3 to avoid shock-wave-induced separation.
- Carefully controlled deceleration along the suction surface from the peak Mach number to avoid turbulent boundary separation ahead of the trailing edge.
- A nearly constant subsonic Mach number distribution on the pressure surface.

Figure 4-10 is a qualitative schematic of the type of Mach number distribution employed. A key feature is to avoid shock wave–boundary layer interaction, such that boundary layer analysis can be used effectively in establishing the desired controlled diffusion characteristic along the suction surface. Initially, inverse techniques, which compute blade geometry from specified Mach number distributions, were used. Once the basic concept was clarified, it became possible to use direct methods to iteratively refine the geometry to achieve the desired aerodynamic characteristics. Typical controlled diffusion profiles (Hobbs and Weingold, 1984) appear to be more robust than the 65-series in the forward portion of the profile, followed by a relatively thin aft region of almost constant thickness. But that is not necessarily a general conclusion. This is really a design concept to produce specific, proprietary profile designs. It has not resulted in a standard airfoil family that can be employed and analyzed in a general sense. Some standardization is clearly possible as evidenced by the fact that controlled diffusion

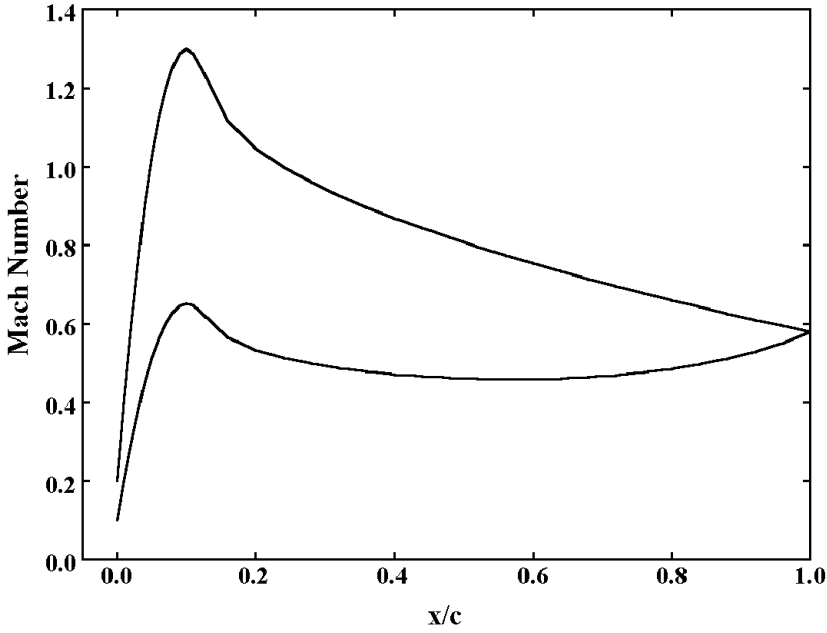

FIGURE 4-10 Controlled Diffusion Airfoil

airfoils have found favor for industrial axial-flow compressors, where unique profile development for each compressor is not economically feasible. But to employ this concept, specific profiles of the desired characteristics must be at least initially designed. And performance prediction models must also be established, since those used for standard profiles are unlikely to be adequate.

4.9 BLADE THROAT OPENING

The blade throat opening, *o*, is the minimum distance between adjacent blades, as illustrated in Fig. 4-11. It is an important parameter when conducting an aerodynamic performance analysis. The throat opening governs the onset of local flow choking within the blade passage. At sufficiently high inlet Mach number levels, this will define the maximum flow capacity that the compressor can pass. The best approach to determine the throat opening is to define adjacent blades using the stagger angle, camberline and profile coordinates to locate the minimum distance between the blades. For that purpose, this writer uses a computer database containing the information in Table 4-1. Then, before an actual performance analysis, the throat openings along the span of all blade rows are computed by a simple trial-and-error process. Typically, about 50 points are distributed along both blade surfaces and the minimum distance is easily located. This process is carried out in the context of a two-dimensional cascade with the correct solidity. The ratio of throat-opening-to-pitch, *o* / *s*, is computed. Conformal mapping shows that this ratio is applicable to the annular cascade of a compressor (e.g., Aungier, 2000, Chapter 7). There is no need to attempt something more sophisticated, since this is a rather trivial problem for a computer.

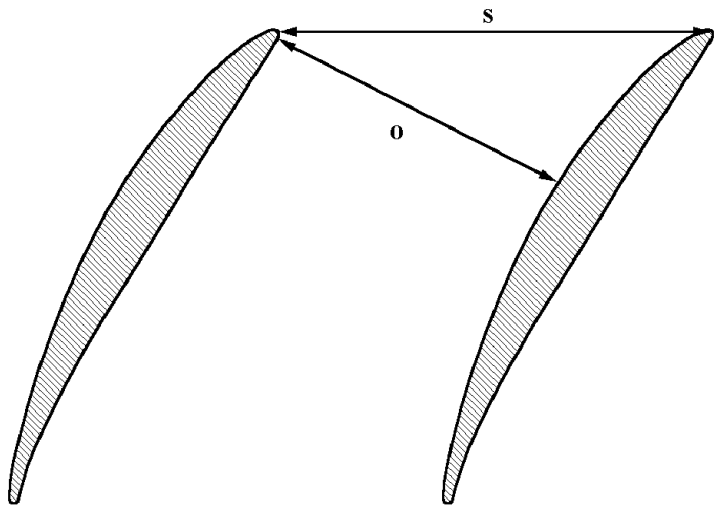

FIGURE 4-11 Throat Geometry

Plus, these data are added to the basic problem input file, so throat openings are only computed once for each compressor to be analyzed. The same process can be used for any blade type, such as the controlled diffusion airfoils discussed in the previous section. It is only necessary to have the camberline and profile coordinates available from a database.

It is also possible to approximate throat openings with reasonable accuracy using an empirical correlation. This writer developed a throat-opening correlation for NACA 65-series blades from the carpet plots of Dunavant et al. (1955). A modified stagger angle parameter, ϕ, is defined as

$$\phi = \gamma(1 - 0.05C_{l0}^{1.5}) + 5C_{l0}^{1.5} - 2 \tag{4-30}$$

and the ratio of throat opening-to-pitch, o / s, is estimated from

$$o / s = [(1 - t_b\sqrt{\sigma} / c)\cos\phi]^{\sqrt{\sigma}} \tag{4-31}$$

Results from this correlation are compared to actual values of o/s for typical NACA 65-series blades in Fig. 4-12. This correlation has been found to be reasonably accurate for other blade types also. As a somewhat extreme example, it is compared to actual throat openings for a C4-series profile that is imposed on a parabolic-arc camberline with a/c = 0.4 in Fig. 4-13. Equation (4-29) was used to

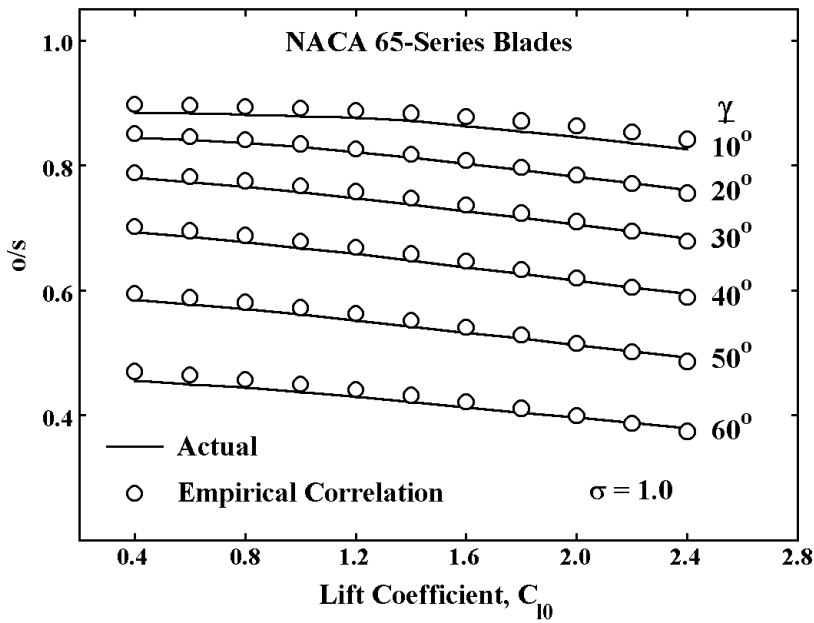

FIGURE 4-12 Throat-Opening Correlation

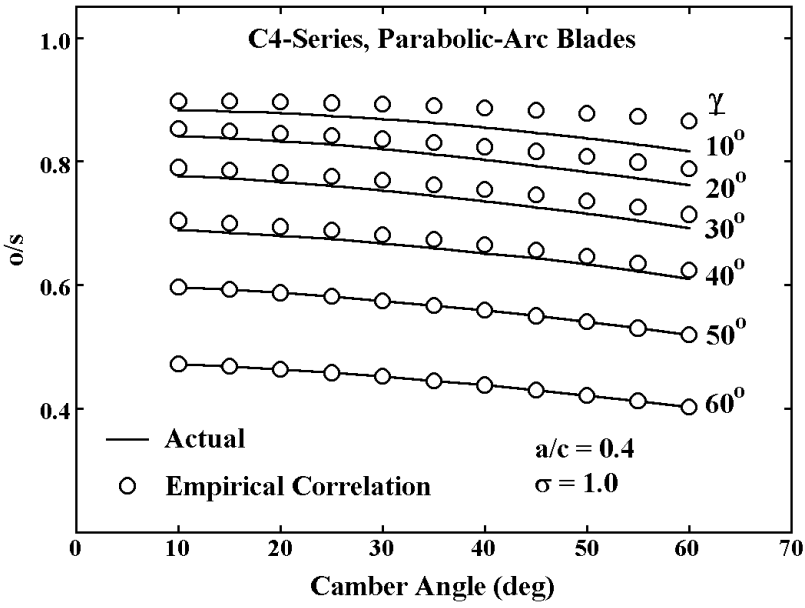

FIGURE 4-13 Extended Throat-Opening Correlation

relate lift coefficient and camber angle for this comparison. While both the profile and camberline are quite different from the NACA 65-series blades for which the correlation was developed, accuracy is still quite good except at very low stagger angles in combination with high camber angles. That small region of inaccuracy is unlikely to be encountered in a real compressor application. Nevertheless, it is prudent to use the actual throat openings for performance analysis applications. This removes the uncertainty as to applicability of the empirical correlation to the specific blades used. It also ensures accurate treatment of special blade types for which the correlation is not likely to apply. A common example is an inlet guide vane row, where the blade throat will normally be located at the trailing edge, similar to a turbine blade row. A compressor blade throat correlation is unlikely to handle this situation accurately. While inlet guide vane choking is not common, it could be a factor if stagger angles are set too high. This could produce an unexpected limit on the compressor's flow capacity unless the problem is handled correctly.

4.10 STAGGERED BLADE GEOMETRY

Once the camberline and profile coordinates for any of the proceeding blade types have been generated along the chord, the geometry of the staggered blade in the cascade is obtained by a simple rotation of coordinates to the stagger angle, γ. The staggered blade inlet and discharge angles are given by

$$\kappa_1 = \chi_1 + \gamma \tag{4-32}$$

$$\kappa_2 = \gamma - \chi_2 \tag{4-33}$$

From Eqs. (4-1), (4-32) and (4-33), it follows that

$$\theta = \kappa_1 - \kappa_2 \tag{4-34}$$

For the circular-arc or the NACA 65-series equivalent circular-arc approximation, it is easily shown that

$$\chi_1 = \chi_2 = \theta / 2 \tag{4-35}$$

$$\gamma = (\kappa_1 + \kappa_2) / 2 \tag{4-36}$$

For the parabolic-arc or equivalent parabolic-arc camberlines, Eqs. (4-17) through (4-19) can be used to compute χ_1 and χ_2 as a function of θ and a/c for use in Eqs. (4-32) through (4-34). Indeed, it is easily shown that the same approach can be used for circular-arc and equivalent circular-arc camberlines, since Eqs. (4-17) through (4-19) are equivalent to Eqs. (4-35) and (4-36) when $a/c = 0.5$.